Characterizing Earth's Surface Using Moderate Resolution 14Ghz Scatterometer Imagery: Early Results from NSCAT Construction

Perry J. Hardin, David G. Long, and Ryan R. Jensen
Microwave Earth Remote Sensing Group, 676 SWKT, Brigham Young University, Provo UT, 84602
Email: perry_hardin@byu.edu, long@ee.byu.edu. Phone: (801) 378-6062

I. INTRODUCTION

Currently there is an extended effort to measure and model global climate. Small-scale vegetation maps, some derived from satellite imagery, are important components of these models. Because of the very large continental regions involved, Advanced Very High Resolution Radiometer (AVHRR) imagery and its derivative vegetation index products with resolutions between 1 and 12 km have been the preferred source material for many of these maps. However, because of persistent cloud cover in many regions critical to global climate such as polar and equatorial areas, active microwave sensors which are sensitive to vegetation and ice variations may be better for this global mapping task than visible and near infrared sensors such as AVHRR.

Scatterometers are active microwave instruments used to measure ocean wind speed and direction. The first spaceborne scatterometer, S-193, flew as part of the Skylab mission in 1973. However, most of what we learned early about spaceborne scatterometers came from the ill-fated flight of Seasat-A. Although the mission lasted only 99 days in 1978 before being catastrophically terminated, the experience gleaned from the Seasat-A scatterometer (SASS) was sufficient to prove that satellite-based scatterometers were invaluable instruments for the study of ocean winds. The launch of ERS-1 in 1991 provided further evidence of the scatterometer's worth. The ERS-1 advanced microwave instrument (AMI), operating in wind scatterometer mode, is capable of land and sea imaging with pixel resolutions of approximately 50 km.

Launched in August 1996, the NASA scatterometer (NSCAT) was also designed to measure ocean wind vectors. However, like its SASS predecessor, NSCAT data is also acquired over land. Though collected at a resolution of 25km, resolution enhancements permit image reconstruction to image cell approaching 8 km. When reconstructed to this moderate resolution, the NSCAT data can be an important addition to AVHRR for global monitoring of cloudy regions. In other words, the scatterometer can be viewed as an active microwave instrument for land and ice imaging, as well as wind assessment.

The purpose of this paper is to report preliminary results of research designed to measure the characteristics of earth's land surface as depicted in reconstructed NSCAT imagery.

II. NSCAT AND IMAGE RECONSTRUCTION

NSCAT measures σ_o over a wide range of incidence angles, at several azimuth angles, and with both horizontal and vertical polarization. The wide swath enables the frequent observation of targets. By combining data from multiple passes with the SIRF algorithm [1,2], enhanced resolution images of the surface backscatter can be made with an effective resolution of 8-10 km. Primarily, the SIRF algorithm provides images of σ_o at a 40° incidence angle (designated ***A***). The algorithm also provides an image of the slope of σ_o versus incidence angle (designated ***B***). While ***A*** images are used more frequently, ***B*** images may prove useful in understanding the scattering mechanisms responsible for the observed backscatter and in discriminating between various land cover types.

III. FIRST IMAGES

Figure 1 is a low-resolution reproduction of a global NSCAT composite (***A***, vertical polarization) for September of 1996. Perhaps the most striking characteristic of the image as a whole is the contrast and detail available in the absence of any significant atmospheric effect.

Figure 2 is a low-resolution reproduction of the United States and Canada. Unlike its early SASS counterpart, the major urban areas such as St. Louis, Kansas City, Chicago, Montreal and several Texas conurbations are clearly visible as bright dots or patches. The boundary between the agricultural heartland (brighter) and the shortgrass prairie (very dark) to the east of the Rocky Mountains is also clearly seen. The boundary between the Canadian taiga and agriculture is also detectable. Besides the urban areas, the brightest areas on the map (which is not an artifact of the imaging process) are the Mojave Desert and southwestern Great Basin.

This high Mojave desert backscatter is in contrast to the low backscatter from the sandy desert in Northern Africa (Figure 3). This stunning depiction of the Northern Africa surficial geology shows the areas of erg, reg, and hamada with different backscatter. The Tibesti Massif appears as a bright gray spot nearly dead-center in the image, whereas the large sand seas such as the Grand Erg Occidental appear as very dark gray patches. The transition from equatorial broadleaf forest through savanna grasslands, to the shrub steppe zone and ultimately to the north African desert is easily recognizable on the NSCAT image as a progression from white to nearly black tones.

0-7803-3836-7/97/$10.00 © 1997 IEEE

Figure 4 is an image of Earth's north polar region. Currently there is an ongoing effort to map the extent and movement of sea ice using reconstructed NSCAT imagery. Two fundamental challenges are being addressed. First is the challenge to distinguish between rough open water and the edge of the ice which borders it. The second is distinguishing between the various phases of the sea ice itself.

Figure 5 is a reconstructed NSCAT image which includes Europe, southwest Asia, and the Mediterranean. Several urban areas are visible on the image. The non-urban tone gradations are largely due to agricultural mosaics and differences in natural vegetation. In the barren tundra areas, the different tones are likely due to moisture content of the soil.

IV. QUANTITATIVE ANALYSIS

In order to better determine the utility of reconstructed NSCAT imagery for actually discriminating between land cover classes and mapping land cover extent and change, a digital version of Matthew's vegetation type map [2] was compared to the NSCAT imagery. Summary backscatter statistics were calculated for each of the 31 vegetation classes represented in the map. The results of this simple analysis, sorted in descending order by A are shown in Table 1. As shown in the table, both ice and equatorial evergreen forest have the highest backscatter of any land cover class. Roughly speaking, backscatter decreases as the density of canopy cover decreases. There are some exceptions. Dense temperate needleleaved backscatter is relatively low compared to its equatorial equivalent.

V. SUMMARY

To a large extent, early research conducted with reconstructed SASS imagery to determine its ability to monitor vegetation at a regional scale has been confirmed by these early examinations of NSCAT imagery. While not a replacement for moderate resolution sensors such as AVHRR, reconstructed NSCAT imagery can be viewed as another primary source of geophysical data over earth's land and ice surfaces. From visual examination of imagery and simple quantitative analysis, there appears to be a relationship between normalized backscatter (A) and variables such as canopy cover, stage of crop growth, bare ground exposure, and moisture.

VI. REFERENCES

1. Long, D.G. and P.J. Hardin (1993) High resolution imaging of land/ice using spaceborne scatterometry part I: the imaging technique. *IEEE Transactions on Geoscience and Remote Sensing*. Vol. 31, No. 3, pp. 700-715.

2. Matthews, E. (1983). *Global Vegetation, Land-Use, and Seasonal Albedo* [NASA Goddard Institute for Space Studies]. Digital Raster Data on a 1-degree geographic (lat / lon) 180x360 grid. Boulder, CO: National Center for Atmospheric Research. 9 track tape, 0.8 mb.

Table 1. NSCAT backscatter summary for global land cover.

Land cover category	Mean A	Standard deviation A
Tropical evergreen forest, mangrove forest	-7.03	1.57
Ice	-7.21	3.73
Tropical / subtropical evergreen seasonal broadleaved forest	-7.41	1.64
Tropical / subtropical evergreen needleleaved forest	-7.92	1.02
Temperate evergreen seasonal broadleaved forest, summer rain	-7.94	1.19
Tropical / subtropical drought - deciduous forest	-8.01	1.78
Tall / medium / short grassland with < 10% woody tree cover or tuft-plant cover	-9.11	2.03
Xeromorphic forest / woodland	-9.18	1.53
Tropical / subtropical drought-deciduous woodland	-9.21	1.58
Tall grassland, no woody cover	-9.25	2.03
Cold-deciduous forest, with evergreens	-9.35	1.44
Tall / medium / short grassland with 10 - 40% woody tree cover	-9.45	1.92
Evergreen broadleaved sclerophyllous forest, winter rain	-9.47	1.39
Cold-deciduous forest, without evergreens	-9.71	1.16
Drought-deciduous shrubland / thicket	-9.89	2.31
Subtropical evergreen forest	-9.90	1.25
Temperate / subpolar evergreen rainforest	-9.90	1.66
Evergreen broadleaved sclerophyllous woodland	-10.00	1.67
Meadow, short grassland, no woody cover	-10.15	2.12
Forb formations	-10.15	1.83
Evergreen broadleaved shrubland / thicket, evergreen dwarf-shrubland	-10.29	2.51
Evergreen needleleaved or microphyllous shrubland / thicket	-10.41	1.31
Temperate / subpolar evergreen needleleaved forest	-10.44	1.02
Evergreen needleleaved woodland	-10.47	1.55
Medium grassland, no woody cover	-10.56	1.74
Cold deciduous woodland	-10.85	1.19
Arctic, alpine tundra, mossy bog	-11.23	1.99
Xeromorphic shrubland / dwarf shrubland	-11.24	2.56
Tall / medium / short grassland with shrub cover	-11.40	2.86
Cold-deciduous subalpine / subpolar shrubland, cold-deciduous dwarf shrubland	-12.30	1.82
Desert	-12.90	4.53

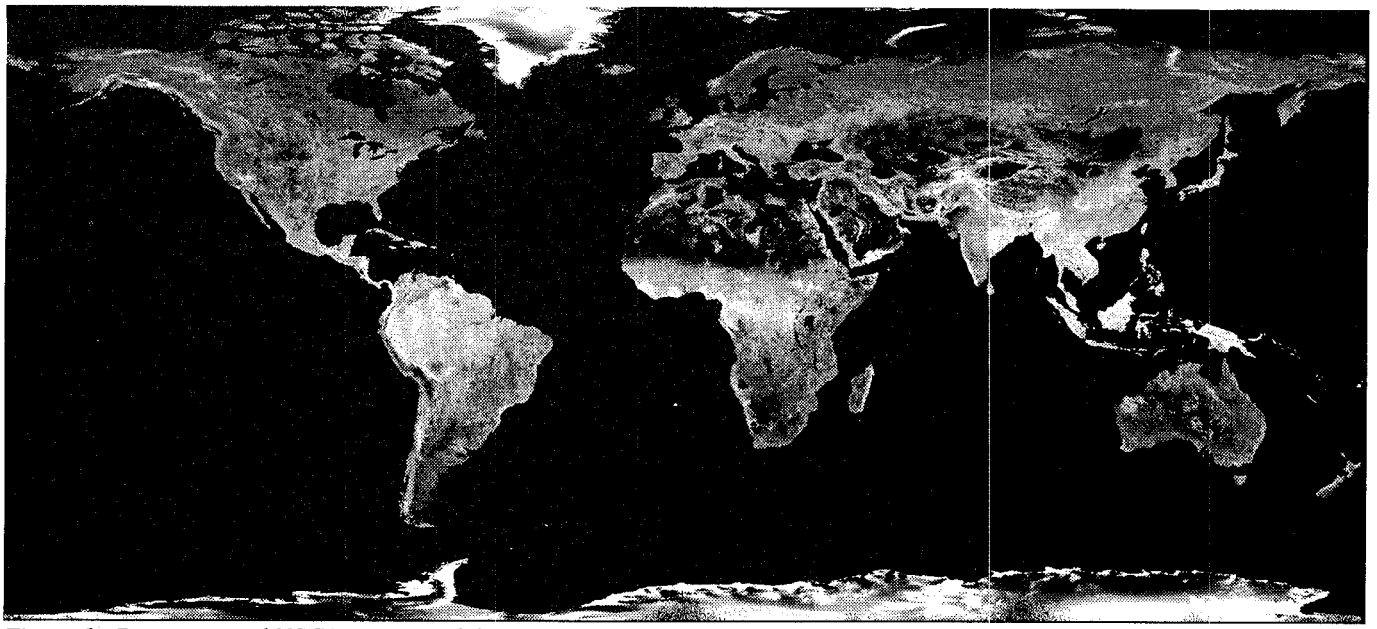

Figure 1. Reconstructed NSCAT image of the earth. September, 1996

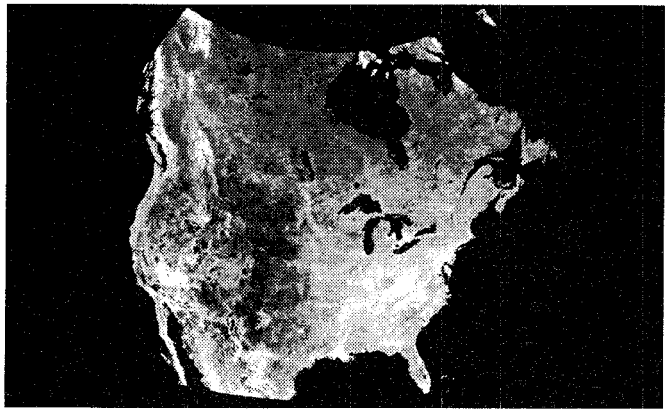

Figure 2. Reconstructed NSCAT image of the continental United States and Canada. Note the bright urban areas.

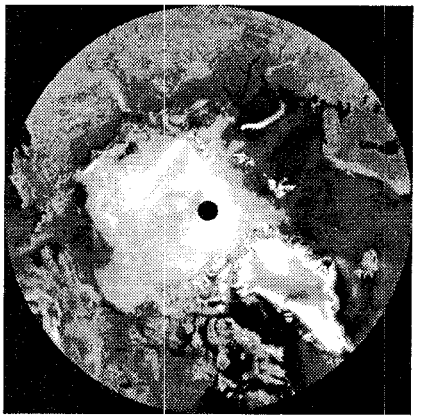

Figure 4. Reconstructed NSCAT image of the North Polar region. September, 1996

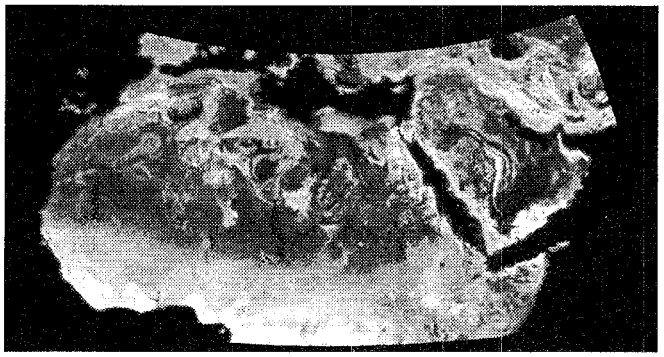

Figure 3. Reconstructed NSCAT image of North Africa, September, 1996.

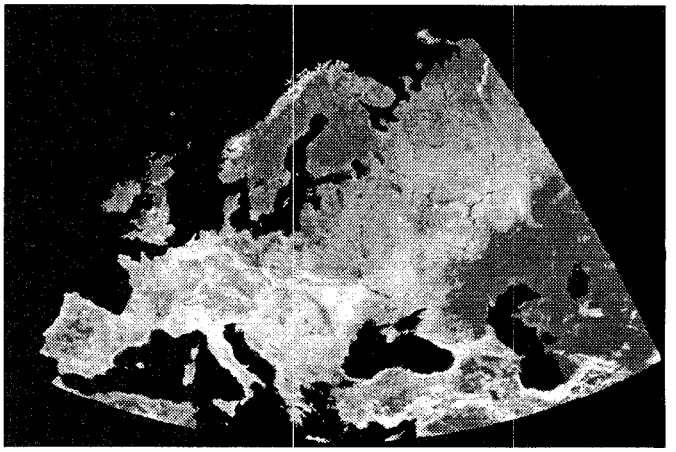

Figure 5. *Reconstructed NSCAT image of Europe and Southwest Asia, September 1996.*